CELL BIOLOGY

Identification of the hyaluronic acid pathway as a therapeutic target for facioscapulohumeral muscular dystrophy

Alec M. DeSimone[1], John Leszyk[2], Kathryn Wagner[3], Charles P. Emerson Jr.[1]*

Facioscapulohumeral muscular dystrophy (FSHD) is linked to epigenetic derepression of the germline/embryonic transcription factor DUX4 in skeletal muscle. However, the etiology of muscle pathology is not fully understood, as DUX4 misexpression is not tightly correlated with disease severity. Using a DUX4-inducible cell model, we show that multiple DUX4-induced molecular pathologies that have been observed in patient-derived disease models are mediated by the signaling molecule hyaluronic acid (HA), which accumulates following DUX4 induction. These pathologies include formation of RNA granules, FUS aggregation, DNA damage, caspase activation, and cell death. We also observe previously unidentified pathologies including mislocalization of mitochondria and the DUX4- and HA-binding protein C1QBP. These pathologies are prevented by 4-methylumbelliferone, an inhibitor of HA biosynthesis. Critically, 4-methylumbelliferone does not disrupt DUX4-C1QBP binding and has only a limited effect on DUX4 transcriptional activity, establishing that HA signaling has a central function in pathology and is a target for FSHD therapeutics.

INTRODUCTION

Facioscapulohumeral muscular dystrophy (FSHD) is a prevalent, debilitating muscular dystrophy without available treatments that arises when *DUX4*, a gene normally restricted to the germ line, mesenchymal stromal cells, and the preimplantation embryo, becomes epigenetically derepressed in the skeletal muscle of affected individuals (*1*–*3*). The DUX4 protein is a double homeobox transcription factor that regulates transcription of a large set of well-defined genes (*4*, *5*). While the exact mechanism whereby DUX4 causes muscle pathology remains uncertain, the prevailing view is that DUX4 activates misexpression of an inappropriate genetic program in muscle, causing pathology and cell death (*1*). DUX4 has been shown to be toxic when misexpressed in a number of FSHD models (*6*–*12*). Cell death appears to be p53 dependent and occurs in part via activation of caspase-3/7, resulting in apoptosis (*6*, *8*, *9*), although recent evidence supports the existence of a p53-independent mechanism (*13*, *14*).

The pathways that trigger DUX4-dependent cell death are currently under investigation. One possible mechanism is increased oxidative stress. Genes that confer resistance to oxidative stress are down-regulated in FSHD cells (*15*), and FSHD subject-derived myoblasts, biopsies, and/or DUX4-expressing cells have higher basal levels of oxidative stress and reactive oxygen species (ROS) (*16*, *17*). DUX4 expression also disrupts additional cellular processes. DUX4-expressing myoblasts have differentiation/fusion defects and misregulation of the myogenic program (*6*, *7*, *11*, *18*) [although some of these observations have not been confirmed (*5*, *19*)] and distorted morphology (*19*, *20*), and DUX4 expression is associated with altered cell migration (*21*). Another possibility is that DUX4 binds to or suppresses expression of myogenic transcription factors PAX3 and PAX7, which are not detected in DUX4-expressing cells, and their overexpression can rescue DUX4 pathology. Suppression of PAX7 target gene expression has been reported as a signature of FSHD muscle (*6*, *22*–*24*). At the molecular level, subject-derived or DUX4-expressing cells also have altered expression of spliceosome components and splicing patterns (*12*), impaired nonsense-mediated decay (*25*), impaired ubiquitination (*26*), and altered proteomes (*18*, *27*). In addition, specific markers of DUX4-induced pathologies include nuclear aggregation of the splicing- and amyotrophic lateral sclerosis (ALS)–associated transactive response DNA binding protein 43 kDa (TDP-43) and fused in sarcoma (FUS) proteins, disrupted promyelocytic leukemia protein (*PML*) bodies and SC35 speckles (*26*, *28*), and the appearance of double-stranded RNA (dsRNA) granules (*14*). These disruptions may be a downstream result of misexpression of DUX4 target genes, or they may be direct results of interactions with cellular proteins, as DUX4 has recently been shown to bind to a wide variety of proteins, including the aforementioned FUS protein (*29*).

To investigate mechanisms underlying of DUX4-induced pathologies, we conducted a proteomics study in FSHD subject-derived cells to identify DUX4-interacting proteins that might place DUX4 expression within a pathway that mediates its toxicity. We found that DUX4 binds C1QBP, an interaction that has also recently been identified in a yeast two-hybrid screen (*29*). C1QBP is regulated by the prevalent glycosaminoglycan hyaluronic acid (HA) both through direct C1QBP-HA binding and by phosphorylation via an HA-dependent signaling pathway (*30*–*32*), suggesting a role for HA-mediated signaling in DUX4-induced toxicity. To examine this possibility, we have used the DUX4-inducible human myoblast cell line MB135-DUX4i (*33*), which has been shown to have molecular disease pathologies similar to those reported in patient-derived FSHD myogenic cells. Unlike FSHD cells, which sporadically express DUX4 in a small fraction of nuclei (*34*, *35*), MB135-DUX4i cells can be synchronously induced to activate high-level expression of DUX4, uniquely enabling molecular investigations of DUX4 pathologies under controlled and acute experimental conditions. Using this model, we demonstrate that DUX4 expression promotes accumulation of HA in DUX4-expressing cells. Furthermore, we show that increased HA levels are associated with multiple previously unobserved cellular pathologies, including disruption of the normally perinuclear localization of C1QBP and the mitochondria, as well as several pathologies that

[1]Wellstone Muscular Dystrophy Program, Department of Neurology, University of Massachusetts Medical School, Worcester, MA, USA. [2]Department of Biochemistry and Molecular Pharmacology, University of Massachusetts Medical School, Worcester, MA, USA. [3]Center for Genetic Muscle Disorders, Kennedy Krieger Institute, Johns Hopkins School of Medicine, Baltimore, MD, USA.
*Corresponding author. Email: charles.emersonjr@umassmed.edu

have previously been observed in FSHD-derived cell lines expressing endogenous DUX4, including induction of nuclear dsRNA foci, FUS aggregation, DNA damage, and cell death. Critically, treatment of DUX4-expressing myoblasts with 4-methylumbelliferone (4MU), a well-characterized competitive inhibitor of HA biosynthesis (*36*), prevents DUX4-induced accumulation of HA and the induction of each of these pathologies, including the activation of caspase-3/7 and cell death. 4MU treatment prevents these pathologies without having an observable impact on DUX4 protein abundance or nuclear localization. Our findings therefore establish HA as an essential mediator of DUX4 pathology that functions at an early stage in DUX4 pathogenesis and identify HA synthesis and HA-dependent pathways as FSHD therapeutic targets.

RESULTS

DUX4 expression causes pathological accumulation of HA

To identify molecular pathways that mediate DUX4 toxicity, we used proteomic coimmunoprecipitation (co-IP) assays and identified C1QBP as a DUX4-interacting protein in FSHD subject-derived cell lines (data S1). C1QBP has also been identified as a DUX4-binding protein in a yeast two-hybrid screen and validated with co-IP and HaloTag pull-down systems (*29*). C1QBP is a promising candidate mediator of DUX4 and FSHD pathology because of its functions in multiple processes that are disrupted in FSHD muscle and/or in response to DUX4 misexpression, both in the nucleus, where it regulates gene expression (*37*, *38*) and RNA splicing [reviewed in (*39*)], and in the mitochondria, where it regulates metabolism (*40*), ROS generation, and cell death/apoptosis (*39*), and it is also a regulator of cell migration (*41*). C1QBP is also regulated by the signaling molecule HA, which it can bind to directly, and its function is subject to HA-regulated signaling cascades (*30*–*32*).

To investigate the role of HA and C1QBP in DUX4-induced cytotoxicity, we used the MB135-DUX4i myoblast FSHD model, an immortalized myoblast line that has been validated for its FSHD biomarker expression and DUX4-induced molecular pathologies. This line has been engineered with a doxycycline (DOX)–inducible DUX4 transgene, making it uniquely suitable for investigations of DUX4-induced molecular pathologies (*33*). To determine whether HA has a role in DUX4-induced pathogenesis, we assayed changes in cellular HA levels following DUX4 induction using biotinylated HA-binding protein (Fig. 1A). Uninduced cells expressed low levels of HA that noticeably increased following DUX4 induction, while parental myoblasts that do not contain the DUX4 expression cassette did not increase HA expression (fig. S1A). Transcriptome analysis (*33*) and reverse transcription polymerase chain reaction (RT-PCR) demonstrated that DUX4 induction caused increased *HA synthase 3* (*HAS3*) expression in MB135-DUX4i myoblasts, but not in parental cells, providing one possible mechanism for the overall increase in HA abundance (Fig. 1B and fig. S1B).

We next asked whether increased HA levels have any effect on the HA-regulated and DUX4-interacting protein C1QBP. Using immunofluorescence assays, we observed that C1QBP is primarily localized in the perinuclear region of MB135-DUX4i and parental MB135 cells, consistent with mitochondrial localization. Its perinuclear localization was disrupted upon DUX4 induction in MB135-DUX4i cells, but not in parental MB135 cells (Fig. 1C and fig. S1C). To determine whether C1QBP is being dislocated from the mitochondria, we colabeled cells with C1QBP antibodies and MitoSpy dye (Fig. 1D). Under uninduced conditions, robust C1QBP staining occurred almost exclusively within the mitochondria, except for a small patch adjacent to nuclei that stained for C1QBP and did not costain with MitoSpy (Fig. 1D, top). Under induced conditions, both C1QBP and the mitochondria became disorganized, and much of its perinuclear staining was lost, although a large fraction of C1QBP staining remains colocalized with the mitochondria (Fig. 1D, bottom), showing that DUX4 expression also disrupts mitochondrial organization. Both C1QBP and the mitochondria remained perinuclear in response to DOX induction in parental MB135 control cells (fig. S1, C and D). To investigate whether C1QBP mislocalization is a secondary response to DUX4-induced activation of caspases and apoptosis, we assayed C1QBP localization in DOX-induced MB135-DUX4i cells in the presence of the caspase-3/7 inhibitor Z-DEVD-FMK. We found that Z-DEVD-FMK inhibited caspase-3/7 activation (fig. S2A) and the appearance of condensed, apoptotic chromatin (fig. S2B) but did not prevent the mislocalization of C1QBP (Fig. 1E). To determine whether mislocalization of C1QBP is an effect of DUX4-induced ROS generation, we treated induced cells with the antioxidant β-mercaptoethanol (βME) at a concentration that inhibits DUX4 toxicity (*6*) and found that βME did not block C1QBP mislocalization (fig. S2C), indicating that C1QBP mislocalization is not a downstream response to DUX4-induced oxidative stress (*6*, *17*). These findings establish that C1QBP dislocation is an early response to DUX4 misexpression and identifies C1QBP and mitochondrial mislocalization as DUX4 pathologies associated with HA production.

To test whether increased HA production is required for C1QBP and mitochondrial mislocalization phenotypes, we treated MB135-DUX4i myoblasts with 4MU, a well-established competitive substrate inhibitor of HA biosynthesis that causes rapid depletion of HA (*36*, *42*). We found that 4MU treatment blocked the accumulation of HA in DUX4-induced cells (Fig. 2A) but did not inhibit the expression of *HAS3* in induced cells (Fig. 2B). Notably, 4MU inhibition of HA production preserved the perinuclear localization of C1QBP in DUX4-induced cells but did not affect the expression or localization of DUX4 itself, demonstrating that C1QBP mislocalization is a downstream response to HA overproduction (Fig. 2C). Similarly, 4MU treatment preserved mitochondrial localization (Fig. 2D), establishing that HA is essential for these DUX4-induced pathologies. To investigate the possibility that HA mediates these pathologies by promoting DUX4-C1QBP physical interaction, we performed DUX4-C1QBP co-IP assays on the nuclear fraction of DOX-induced MB135-DUX4i myoblasts in the presence and absence of 4MU. Our findings show that the DUX4-C1QBP complex is not disrupted in response to 4MU depletion of HA (Fig. 2E), suggesting that the critical role of HA in DUX4-induced pathology is not to promote to formation of C1QBP-DUX4 complexes.

Preventing HA production rescues DUX4-induced toxicity

We then investigated whether HA synthesis is required for DUX4-induced cytotoxicity. After 24 hours of DUX4 induction and 4MU treatment, MB135-DUX4i myoblasts showed a marked dose-dependent resistance to cytotoxicity, as evidenced by the reduction in the number of rounded and/or detached cells (Fig. 3A). In addition, while the DUX4-induced cells that remained attached showed atypical, jagged morphology, 4MU-treated cells did not show these changes, instead maintaining a more normal but somewhat elongated shape (likely a result of the absence of secreted HA affecting the

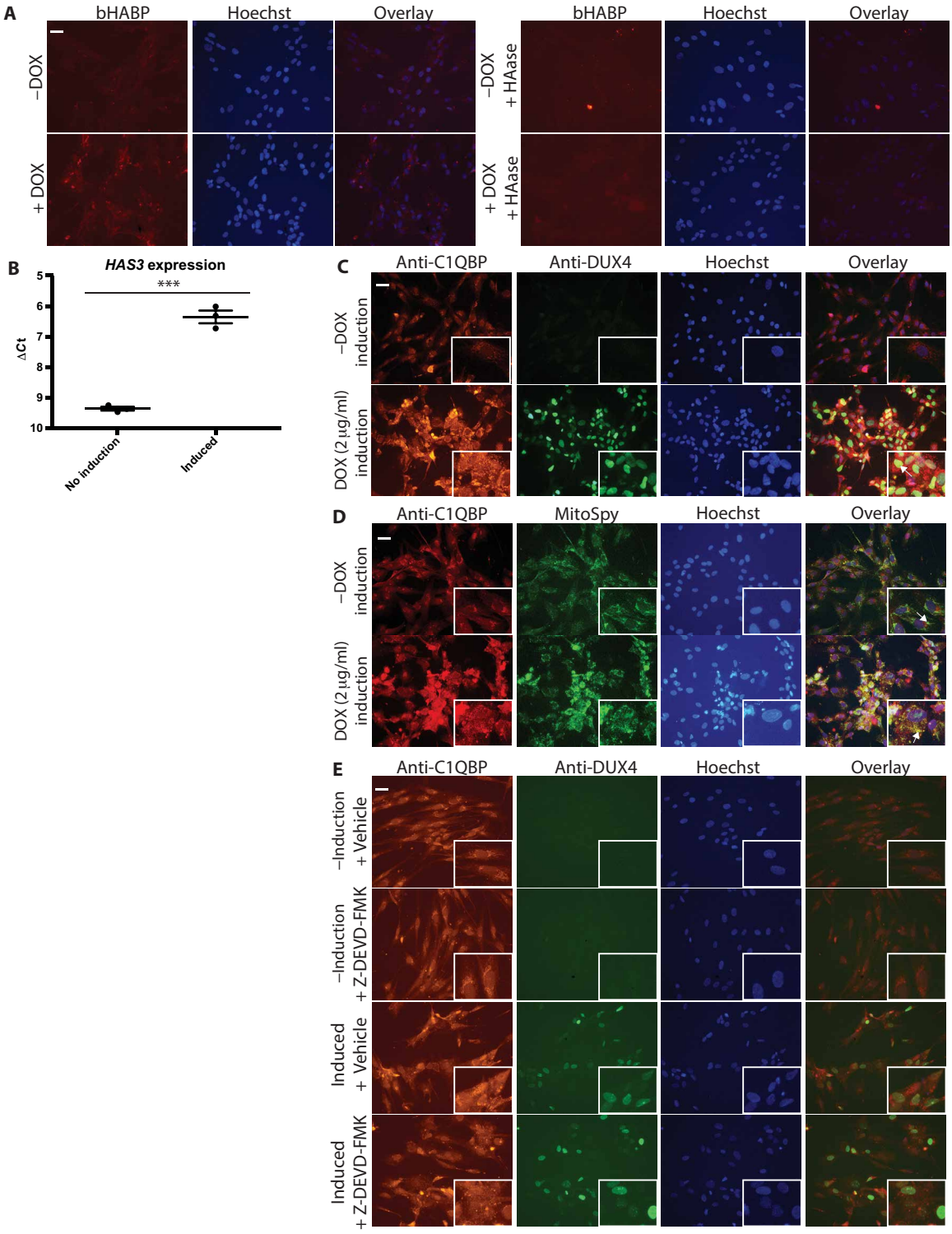

Fig. 1. DUX4 expression causes HA accumulation. (**A**) MB135-DUX4i myoblasts were left untreated or treated with DOX (2 μg/ml) for 24 hours and stained with biotinylated HA-binding protein (bHABP) and Hoechst dye. Control samples were treated with hyaluronidase (HAase) to show specificity of the biotinylated HA-binding protein stain. (**B**) MB135-DUX4i myoblasts were treated as in (A), and the expression of *HAS3* was measured by RT-PCR. The mean ± SEM are indicated. Significance was determined using *t* tests. $n = 3$. (**C**) MB135-DUX4i myoblasts were left untreated or treated as in (A) and immunostained with C1QBP and DUX4 antibodies and Hoechst dye. The arrow indicates examples of overlapping staining. (**D**) Myoblasts were treated as in (A) and stained with C1QBP antibodies and MitoSpy and Hoechst dyes. Arrows indicate examples of overlapping staining. (**E**) Myoblasts were either left uninduced or induced with DOX, treated with 30 μM Z-DEVD-FMK or dimethyl sulfoxide (DMSO) vehicle, and immunostained with C1QBP and DUX4 antibodies and Hoechst dye. Scale bar, 35 μm. Inset: 75 μm. All experiments were performed a minimum of three times. ***$P < 0.001$.

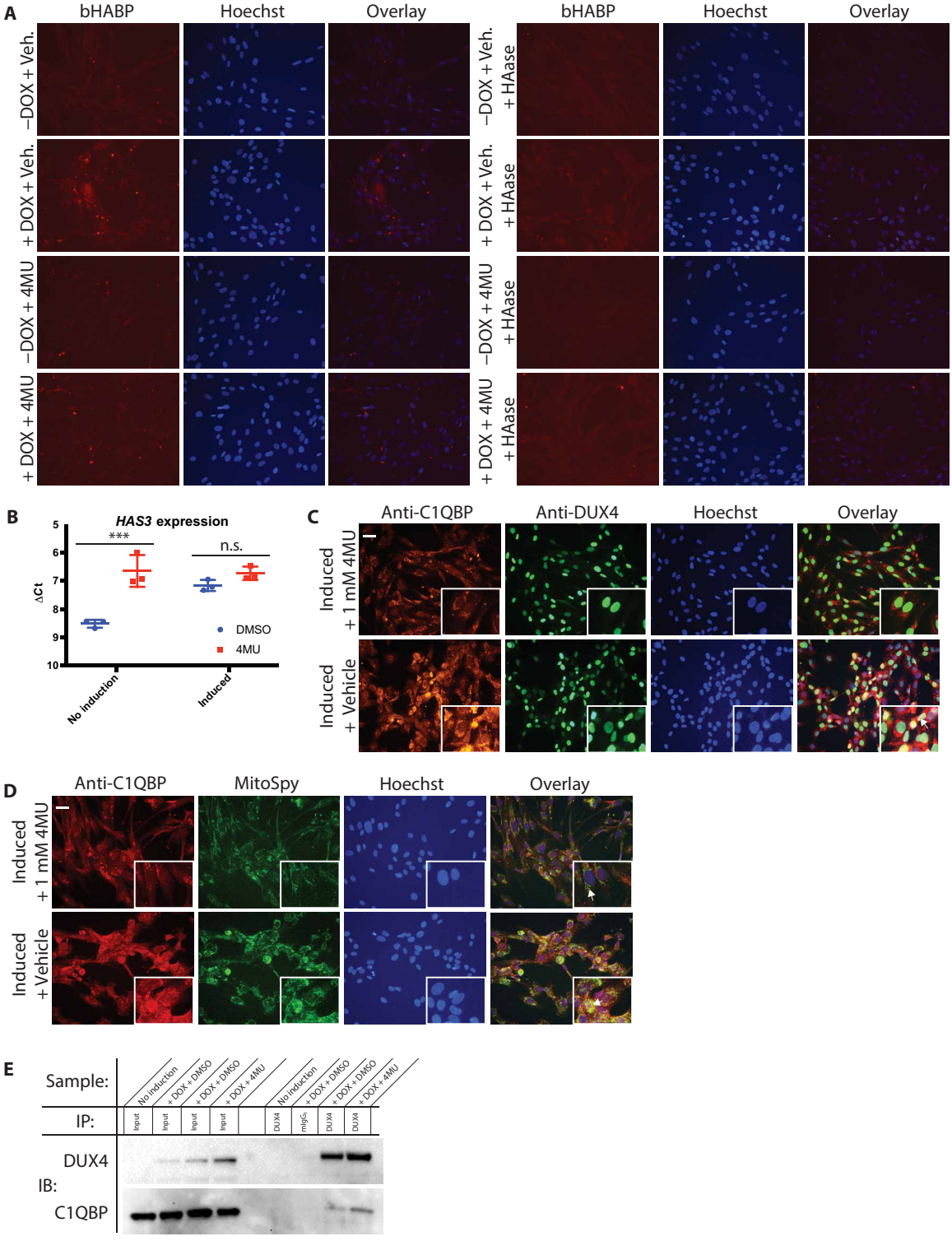

Fig. 2. C1QBP and mitochondrial pathology depend on HA synthesis. (**A**) MB135-DUX4i myoblasts were left uninduced or induced with DOX, simultaneously treated with 1 mM 4MU or 1% DMSO vehicle for 24 hours, and stained with biotinylated HA-binding protein and Hoechst dye as in Fig. 1. (**B**) *HAS3* expression was measured by RT-PCR in uninduced or 24 hour–induced myoblasts treated with 2 mM 4MU or an equal volume of DMSO vehicle. The means ± SEM are indicated. Significance was determined using *t* tests with multiple hypothesis correction using the Bonferroni-Dunn method. $n = 3$. (**C**) Myoblasts were induced, treated with 4MU or DMSO vehicle as in (A), and stained for C1QBP and DUX4 as in Fig. 1C. The arrow indicates examples of overlapping staining. (**D**) Cells were treated as in (C) and stained for C1QBP and mitochondria as in Fig. 1B. Arrows indicate examples of overlapping staining. Scale bar, 35 μm. Inset: 75 μm. (**E**) MB135-DUX4i myoblasts were either left uninduced or induced and treated with the indicated compounds as above. Immunoprecipitations (IP) were performed from nuclear lysates using either DUX4 antibodies or isotype-matched control antibodies, and DUX4 and C1QBP were analyzed by immunoblotting (IB). All experiments were performed a minimum of three times. ***$P < 0.001$, n.s., not significant.

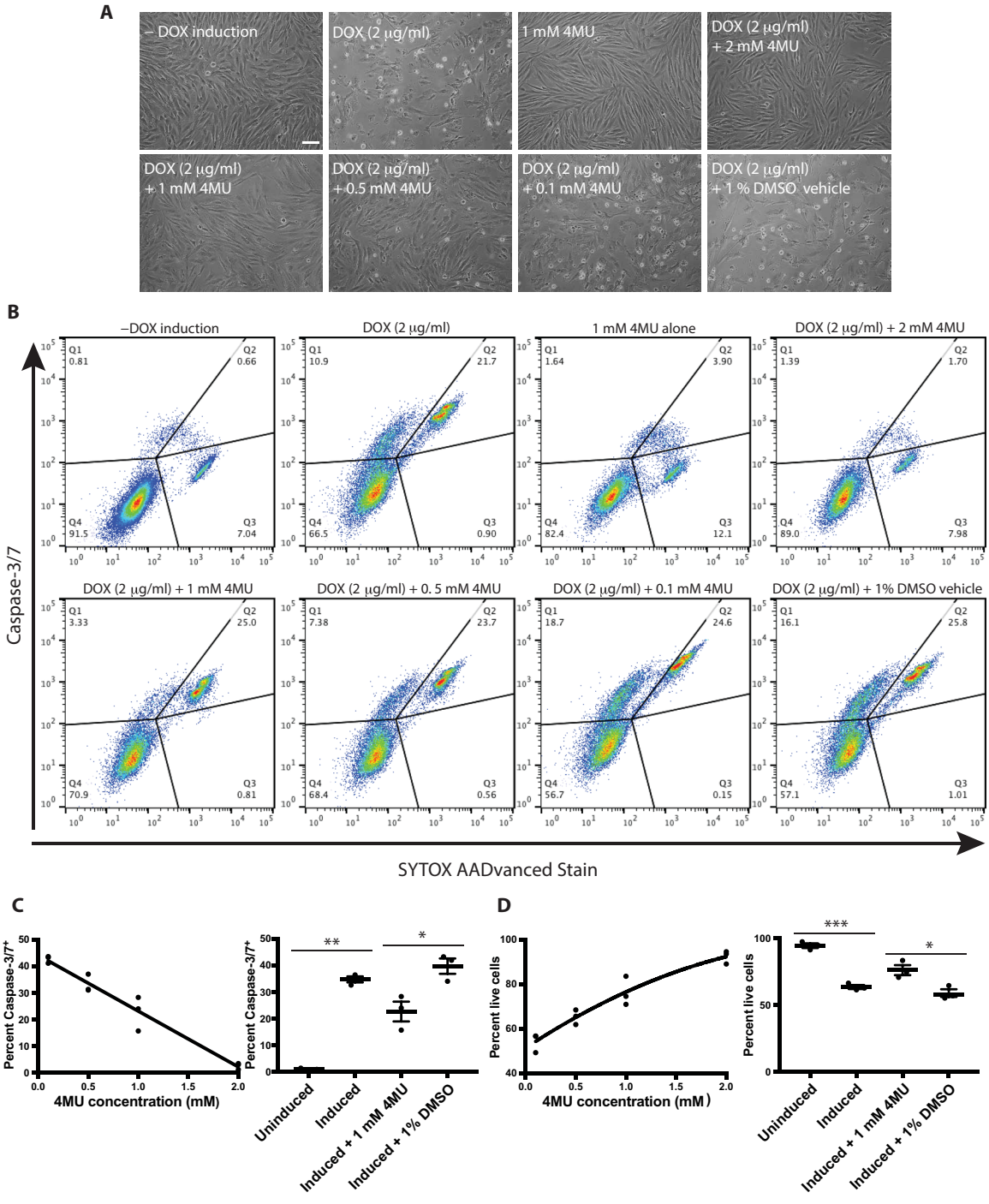

Fig. 3. DUX4-induced toxicity requires HA. (**A**) Myoblasts were left untreated, treated with DOX (2 μg/ml) alone, 1 mM 4MU alone, or DOX (2 μg/ml) plus the indicated concentration of 4MU or DMSO for 24 hours and were imaged by phase-contrast microscopy. Experiments were performed three times. (**B**) Representative scatterplots of flow cytometry experiments. Cells were treated as in (A) and were then stained for caspase-3/7 activation and cell death using the CellEvent Assay Kit. (**C**) Left: The total fraction of caspase-3/7–activated cells (quadrants 1 and 2) from three independent experiments was plotted against the concentration of 4MU used and fitted to a linear trend line. Data points from individual experiments are indicated with dots. $n = 3$. Right: The fraction of caspase-3/7–activated cells from induced myoblasts treated with 1 mM 4MU plotted against induced myoblasts treated with an equal volume (1%) of DMSO. Values from individual experiments are indicated with dots. The means ± SEM are indicated. $n = 3$. (**D**) Left: As in (C), with the total fraction of live cells (quadrant 4) plotted against the concentration of 4MU and fitted to a second-degree polynomial trend line. Right: The fraction of live cells from induced cultures treated with 1 mM 4MU plotted against induced cultures treated with an equal volume (1%) of DMSO. Data points, mean, and SEM are indicated as in (C). Significance was determined using Welch's *t* tests. $n = 3$. Scale bar, 100 μm $^*P < 0.05$, $^{**}P < 0.01$, and $^{***}P < 0.001$.

ability of the cells to attach to the plate). Single-dose treatment with 4MU also provided dose-dependent inhibition of toxicity at 36 and 48 hours following induction (fig. S3, A and B), although less protection was observed at these later time points.

To quantitate the extent of protection that 4MU provides against DUX4-induced toxicity, we used the CellEvent Caspase-3/7 Green Flow Cytometry assay, which measures caspase-3/7 activation and cell permeability to SYTOX stain, a marker of cell death (Fig. 3B). Uninduced cells could be grouped into two distinct populations. Most uninduced cells were negative for both caspase-3/7 activation and SYTOX, reflecting a population of mostly live, nonapoptotic cells. The uninduced cultures also contained a small population of SYTOX-stained, likely necrotic, cells. By contrast, after 24 hours of induction, cells could be assigned to three distinct populations. While many cells remained negative for both caspase-3/7 activation and SYTOX, DOX-induced cultures also contained populations of caspase-3/7–positive cells, as well as a caspase-3/7– and SYTOX double-positive populations. Critically, 2 mM 4MU treatment maintained DOX-induced cultures at low levels of caspase-3/7 and SYTOX staining that were similar to uninduced control cultures, and 4MU inhibition of cell death was dose dependent, as seen in plots of 4MU concentration against the total fraction of caspase-3/7–positive cells (quadrants 1 and 2 of the scatterplots) (Fig. 3C, left) or the fraction of live cells (quadrant 4) (Fig. 3D, left). Results were statistically significant compared to the vehicle control (Fig. 3, C and D, right), which did not affect toxicity, although higher doses of dimethyl sulfoxide (DMSO) had a protective effect (fig. S3, C and D). These results show that preventing DUX4-induced HA accumulation by treatment with 4MU protects cells from the proapoptotic/pro-cell death effects of DUX4 expression, further establishing an essential role for HA as an effector of DUX4-induced cytotoxicity.

4MU blocks DUX4-mediated nuclear pathologies

In addition to DUX4-mediated cell death, a number of DUX4-induced nuclear pathologies have been observed in patient-derived cells expressing endogenous levels of DUX4, suggesting that they are highly relevant to DUX4-induced muscle disease. These include the induction of dsRNA foci, which have been proposed to activate a toxic innate immunity response (*14*), the misregulation of the ALS-associated nuclear protein FUS into large aggregates and discreet foci (*28*), and the accumulation of DNA damage (*16*, *43*). To determine whether HA signaling is important to these pathologies, we used immunostaining assays and 4MU to investigate their dependence on HA. Using the K1 antibody, which specifically recognizes dsRNA foci, we found that inducing cells with DOX led to the appearance of these dsRNA foci in MB135-DUX4i myoblasts (Fig. 4A), but not in parental myoblasts (fig. S4A). The appearance of these foci was blocked by 4MU (Fig. 4A), showing that DUX4-induced dsRNA granule formation is dependent on HA accumulation. To determine whether the HA requirement is specific to DUX4 pathology or a general requirement of HA for foci formation, we induced dsRNA foci by transfection of myoblasts with polyinosinic:polycytidylic acid [poly(I:C)], followed by treatment with 4MU or vehicle control, and we found that 4MU did not block poly(I:C) induction of dsRNA foci (Fig. 4B). These findings establish that the requirement for HA synthesis in foci formation is specific to DUX4-induced foci and unrelated to the downstream process of foci formation.

We next investigated the effect of 4MU on the DUX4-induced redistribution of the FUS protein (*28*). After 24 hours of induction, we observed DUX4-specific appearance of dysregulated FUS in the form of uneven/aggregated staining, discreet foci, and low-level staining, but this was not observed in parental cells (Fig. 4A and figs. S4B and S5). 4MU treatment reduced the prevalence of these disruptions (Fig. 4A and fig. S5). Unexpectedly, we observed that FUS foci often colocalized with dsRNA foci. We quantitated these observations by counting the fraction of nuclei containing at least one dsRNA focus and the fraction of dsRNA foci that colocalize with a FUS aggregate,and found that approximately 1 in 10 DUX4-induced nuclei contained dsRNA foci and that approximately three-fourths of dsRNA foci colocalize with a FUS aggregate, suggesting that these nuclear body structures arise as part of a common pathological process that depends on HA (Fig. 4, C and D).

The unexpected accumulation of dsRNA and FUS into coaggregates in response to DUX4 induction prompted us to investigate whether these granules are associated with double-stranded DNA (dsDNA) breaks, as both FUS and dsRNA have been associated with DNA repair (*44*, *45*), and DUX4 expression is known to cause DNA damage in FSHD subject-derived cells (*16*, *43*). To assay DNA repair, MB135-DUX4i myoblasts were costained with either dsRNA or FUS antibodies and with antibodies to γH2A.X, a histone variant that is a nuclear marker for dsDNA break repair (*46*). We observed increased γH2A.X staining in response to DOX induction in MB135-DUX4i myoblasts, but not in parental myoblasts (Fig. 5A and fig. S4C). γH2A.X staining was reduced in the presence of 4MU, further supporting a requirement for HA in DUX4 DNA damage pathology. Both dsRNA foci (Fig. 5A) and FUS aggregates (fig. S5A) frequently colocalized with γH2A.X foci. We quantitated the fraction of nuclei with dsRNA foci (Fig. 5B) and the fraction of foci colocalizing with γH2A.X (Fig. 5C) and found that greater than half of dsRNA foci were associated with a γH2A.X foci, consistent with a role for these foci in DNA damage repair. Unexpectedly, however, these dsRNA/FUS/γH2A.X foci do not arise purely in response to DNA damage, as DNA damage induced by either hydrogen peroxide or etoposide did not promote dsRNA foci formation (Fig. 5, D and E, and fig. S6, A and B). These findings establish that dsRNA foci are induced by a DUX4-dependent mechanism independent of DNA damage and repair. Similarly, treating induced cells with high concentrations of βME to reduce oxidative stress had only a minimal impact on the number of DUX4-induced dsRNA foci (fig. S7), further validating the conclusion that dsRNA foci formation is a direct response to DUX4. We also observed that 4MU treatment of DUX4-induced myoblasts reduced γH2A.X staining in immunofluorescence assays (Fig. 5A), indicating that DNA damage is an additional DUX4-induced pathology dependent on HA. To validate this finding, we quantitated γH2A.X levels in induced MB135-DUX4i myoblasts by flow cytometry and found that 1 mM 4MU reduced the fraction of myoblasts with dsDNA breaks relative to untreated or vehicle-treated myoblasts (Fig. 5F and fig. S6C), supporting our previous findings that HA is essential for DUX4-induced DNA damage.

HA is not essential for DUX4 transcriptional activity

DUX4-induced pathologies have been proposed to depend on its transcriptional function, as mutations to either its DNA binding domains or its C-terminal domain ablate much of its toxicity (*8*, *10*, *22*). To clarify the role of DUX4-induced transcription in toxicity, we treated either uninduced control or induced MB135-DUX4i myoblasts with 4MU and assayed the expression of *C1QBP* and seven validated DUX4 target genes using RT-PCR (Fig. 6). In uninduced cells, 4MU had an inhibitory effect on the expression of

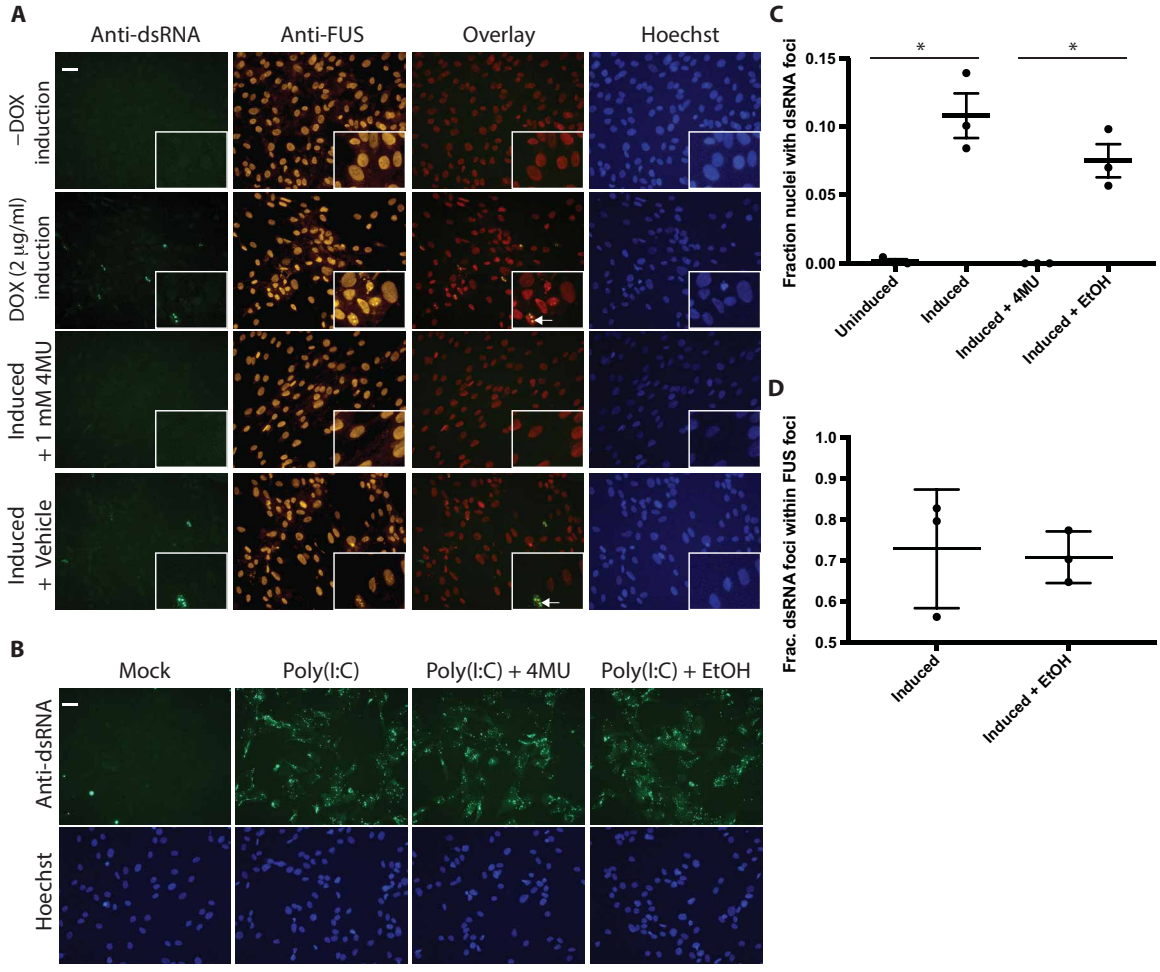

Fig. 4. Nuclear DUX4-induced pathologies are dependent on HA. (**A**) MB135-DUX4i myoblasts were treated with the indicated compounds for 24 hours and stained with antibodies against dsRNA and FUS and with Hoechst dye. (**B**) Myoblasts were transfected with 0.25 μg of poly(I:C) followed by exposure to the indicated compounds for 13 hours and were then stained with dsRNA antibodies and Hoechst dye. Experiments were performed four times. (**C**) The fraction of nuclei containing at least one dsRNA focus was quantified. Significance was determined using Welch's *t* tests with multiple hypothesis correction using the Bonferroni-Dunn method. $n = 3$. (**D**) The fraction of dsRNA foci colocalizing with FUS aggregates was quantified. Values from individual experiments are indicated with dots, and bars indicate the mean of experiments ± SDs. A total of 718 uninduced, 650 induced, 859 induced, 4MU-treated, and 696 induced, ethanol-treated cells were counted among three independent experiments. A total of 290 and 188 dsRNA foci were counted in induced and induced, ethanol-treated cells, respectively. Scale bar, 35 μm. Inset: 75 μm. *$P < 0.05$.

C1QBP and the basal expression of DUX4 target genes. In DUX4-induced myoblasts, 2 mM 4MU selectively inhibited target gene expression. Some targets (*LEUTX*, *KHDC1*, and *MBD3L2*) showed considerable inhibitory effects, while others showed little or no effect (*TRIM43* and *ZSCAN4*), and others showed intermediate effects (*PRAMEF1* and *PRAMEF2*). Even the most 4MU-affected genes were still robustly induced relative to their expression in uninduced cells, even at a high 4MU concentration that completely blocked DUX4-induced cytotoxicity (Fig. 3). These findings establish that 4MU can partially uncouple DUX4 transcriptional activity from DUX4-induced pathology, suggesting that DUX4 toxicity is mediated either by a transcription independent mechanism or by a smaller subset of critical DUX4-regulated genes that mediate its toxicity by activating HA-dependent pathways.

DISCUSSION

In this study we have investigated molecular pathways of DUX4 toxicity using the DUX4-inducible MB135-DUX4i cell model of FSHD pathology (*33*). We observed a number of previously unidentified molecular pathologies that arise from expression of DUX4 in myogenic cells, including changes in localization of the DUX4- and HA-binding protein C1QBP, and misregulation of the mitochondria. We also observed that DUX4 expression induces aberrant accumulation of HA, possibly by increasing expression of the HA-producing gene *HAS3* (*33*) [although the role of HAS3 remains unclear, as virally induced expression of DUX4 in myoblasts led to only a mild up-regulation of *HAS3* expression (*33*) and *HAS3* up-regulation was not observed in DUX4-expressing myotubes (*12*, *33*)]. However, 4MU inhibition of HA synthesis prevents these pathologies, including DUX4-induced pathologies that have been previously observed in FSHD patient cells expressing endogenous levels of DUX4, validating the relevance of these observations to FSHD pathology. Last, we show that inhibiting HA synthesis has little effect on activation of DUX4 target genes or the DUX4-C1QBP complex, which establishes that HA signaling plays an essential role in mediating DUX4-induced pathology.

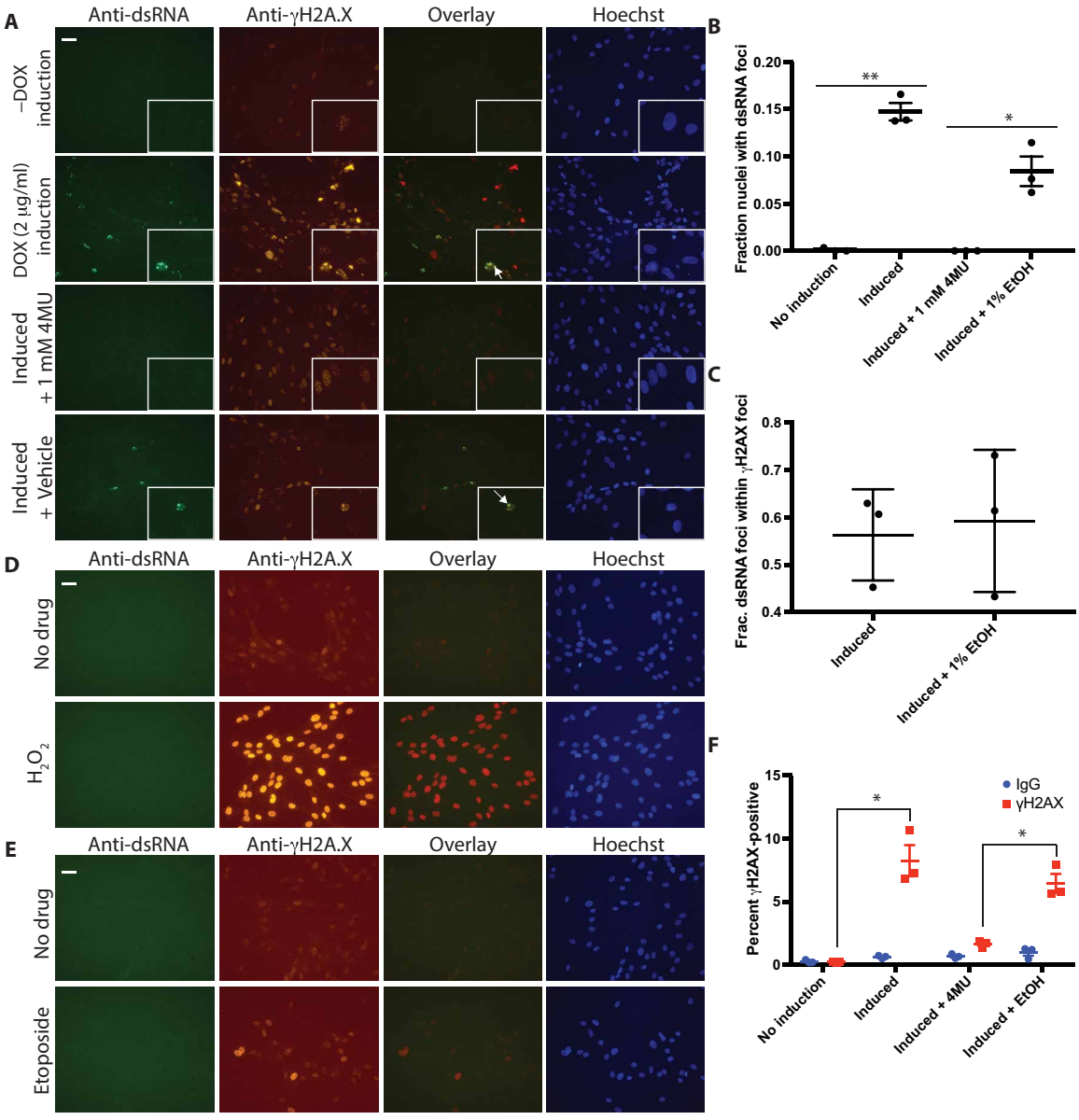

Fig. 5. dsDNA breaks and dsRNA foci appear in response to DUX4. (**A**) Myoblasts were treated as indicated for 24 hours and stained with dsRNA and γH2A.X antibodies and Hoechst dye. Arrows indicate examples of overlapping staining. (**B** and **C**) dsRNA/γH2A.X colocalization was quantitated as in Fig. 3 (C and D). A total of 786 uninduced, 700 induced, 677 induced, 4MU-treated, and 821 induced, ethanol-treated cells were counted among three independent experiments. A total of 381 and 243 dsRNA foci were counted in induced and induced, ethanol-treated cells, respectively. No dsRNA foci were detected in uninduced or induced, 4MU-treated cells. (**D** and **E**) MB135-DUX4i myoblasts were treated with 500 μM H_2O_2 or 20 μM etoposide for 1 hour and stained as in (A). (**F**) Myoblasts were left uninduced, induced for 24 hours or induced and treated with either 1 mM 4MU or 1% EtOH for 24 hours, fixed, labeled with fluorescein isothiocyanate–conjugated control or γH2A.X antibodies, and analyzed by flow cytometry. All experiments were performed at least three times. For (B) and (F), values from individual experiments are indicated with dots, and means ± SEM are indicated with bars. For (C), means and SDs are shown. Significance was determined using Welch's *t* tests. $n = 3$. All experiments were performed at least three times. Scale bar, 35 μm. Inset: 75 μm. *$P < 0.05$ and **$P < 0.01$.

While the precise molecular mechanisms underlying the role of HA in pathology are not yet known, our findings establish that HA has an essential role in DUX4-induced pathology. Inhibition of HA synthesis protects against a diverse array of DUX4-induced pathologies, including disruptions of both nuclear and mitochondrial processes. The observation that these disparate DUX4-dependent pathologies are profoundly inhibited by 4MU indicates that HA acts at a very early step in pathogenesis. An attractive possibility is that HA activates inappropriate signaling pathways that may be toxic to myogenic cells. A second possibility is that HA promotes pathology by directly interacting with protein factors. C1QBP is likely one such HA-binding protein, as it regulates several nuclear and mitochondrial activities affected by DUX4 (*37*–*40*), binds DUX4 [this study and (*29*)], is an HA-binding/HA-regulated protein (*30*–*32*), and becomes dysregulated in DUX4-expressing cells. However, co-IP studies eliminate the possibility that HA is necessary for DUX4-C1QBP binding (Fig. 2E).

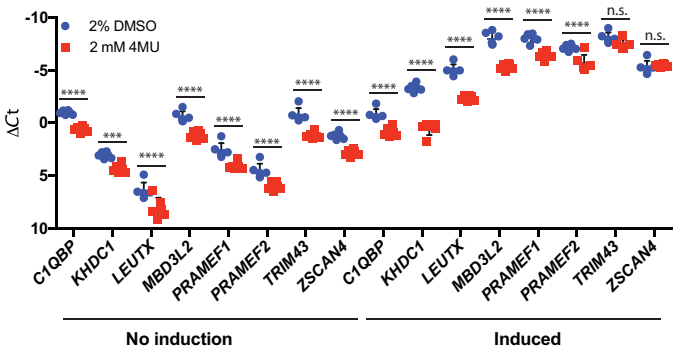

Fig. 6. Effects of HA depletion on DUX4 transcriptional Activity. Uninduced or induced MB135-DUX4i myoblasts were treated with 2 mM 4MU or 2% DMSO for 24 hours, and the expression of C1QBP and seven validated DUX4 target genes was measured by RT-PCR. Values from six independent experiments are indicated with dots and boxes. Means ± SEM are indicated with bars but are concealed by the individual data points for many samples. Significance was determined using *t* tests and multiple hypothesis correction was performed with the Bonferroni-Dunn method. $n = 6$. ***$P < 0.001$ and ****$P \leq 0.0001$.

Alternatively, HA may regulate other functions of C1QBP, or HA signal transduction pathways may mediate pathology. C1QBP also binds to the closely related DUX4c transcription factor (*29*), which is more widely expressed than DUX4 and is also up-regulated in FSHD (*47*), providing a second avenue for changes in HA concentration to trigger pathogenic processes. Thus, by modulating the function of DUX4 and/or DUX4c transcription factors, it is possible that changes in HA abundance may feedback on C1QBP activity, resulting in further perturbation of gene expression or splicing isoform usage. Molecular and biochemical studies of C1QBP that discriminate between these possibilities will be needed to clarify its function as a mediator of the pathological role of HA and as a target for FSHD drug development.

The dependence of DUX4-induced pathology on HA makes its biosynthesis and/or HA-dependent signaling pathways critical targets for the development of FSHD therapeutics. 4MU itself is a potential FSHD therapeutic, as it is an approved drug in Europe for an unrelated indication [reviewed in (*36*)]. 4MU applications for FSHD will require animal model studies to evaluate its known effects on myogenesis (*42*)], which are now feasible (*48*) and will be an important next step. An alternative to inhibiting the production of HA pharmacologically is targeting the HA synthase enzymes, including HAS3, for silencing with antisense oligonucleotide–based approaches combined with adenoviral or chemical delivery systems that target skeletal muscle. In addition, several well-studied signal transduction cascades are induced in response to HA, including RAS phosphorylation, phosphatidylinositol 3-kinase/pyruvate dehydrogenase kinase 1/Akt, and nuclear factor κB pathways, among others (*49*). Determining whether these pathways play a role in toxicity may provide additional targets for FSHD therapeutic development.

MATERIALS AND METHODS

Cell culture

The inducible DUX4 myoblast model MB135-DUX4i and its parental cells (*33*) were provided by S. Tapscott. The line was routinely tested for mycoplasma contamination by the provider. We confirmed identity by ability to induce DUX4 expression and ability to form myotubes and confirmed that it is not present in the Register of Misidentified Cell Lines. 15ABicCT, 15BBicCT, and 15VBicCT immortalized human myoblasts were provided by W. E. Wright (*50*). We confirmed their identity by confirming their ability to form myotubes and by the induction of DUX4 target genes in appropriate cell lines after formation of myotubes, and they were not present in the Register of Misidentified Cell Lines. We confirmed that all five lines are free of mycoplasma contamination. All cells were grown on vessels precoated with 0.1% gelatin (G939, Sigma-Aldrich). MB135-DUX4i and parental myoblasts were propagated in 20% characterized fetal bovine serum (FBS; SH30071.03, Hyclone), dexamethasome (51 ng/ml; D2915, Sigma-Aldrich), fibroblast growth factor-basic (bFGF, 10 ng/ml; GF003AF-MG, EMD Millipore), and 1× antibiotics/antimycotics (30-004-CI, Corning) in Ham's F10 medium (10-070-CV, Corning). 4MU (M1381, Sigma-Aldrich) was diluted in the appropriate culture media from a 100 mM stock in DMSO or 100% ethanol. DUX4 was induced by adding doxycycline (DOX) hyclate (D9891, Sigma-Aldrich) to 2 μg/ml from a stock (2 mg/ml) in water. H_2O_2 (216763, Sigma-Aldrich), βME in phosphate-buffered saline (PBS; 2020-05-30, Gibco/Life Technologies), and etoposide were added to the media at the concentrations indicated. These immortalized, patient-derived myoblasts were grown in medium consisting of 15% characterized FBS, zinc sulfate (0.3 μg/ml; Z0251, Sigma-Aldrich), vitamin B12 (1.4 μg/ml; V2876, Sigma-Aldrich), dexamethasome (3.5 to 54 ng/ml; D2915, Sigma-Aldrich), human hepatocyte growth factor (2.5 ng/ml; 130-093-872, Miltenyi Biotec), bFGF (10 ng/ml), 1× antibiotics/antimycotics (30-004-CI, Corning), and 20 mM Hepes (25-060-Cl, Corning) in medium X [4:1 mixture of Dulbecco's modified Eagle's medium:Medium 199 (10-013-CV and 10-060-CV, Corning)].

Transfections

Plasmid and poly(I:C) transfections were performed using minor modifications to the manufacturer's protocol. One hour before transfection, fresh medium was added to cells. Plasmid or High Molecular Weight poly(I:C) (tlrl-pic, InvivoGen) and Lipofectamine 2000 (11668027, Thermo Fisher Scientific) were diluted separately into Opti-MEM, vortexed briefly, and incubated at room temperature for 5 min. The two solutions were mixed, vortexed briefly, and incubated at room temperature for 20 min. Complexes were added dropwise to cells and placed in the incubator for 5 hours. Medium was then replaced with medium containing the indicated compounds.

Gene expression analysis

RNA was extracted using an RNeasy Mini Kit (74106, Qiagen) according to the manufacturer's instructions, with QIAshredder homogenization and on-column deoxyribonuclease I digestion. Complementary DNA (cDNA) was synthesized using up to 1 μg of RNA and a SuperScript III First-Strand synthesis kit (18080-051, Invitrogen). Reactions were double-primed with oligo dT and random hexamers, but otherwise the manufacturer's protocol was followed, and the optional ribonuclease H digestion was included. Real-time PCR was performed on approximately 30 ng of cDNA using an iQ SYBR Green SuperMix (170-8882, Bio-Rad) and a Bio-Rad CFX96 Real-Time System with the following program: 20-μl volume, 105°C lid temperature, 95°C initial denaturation for 2 min, followed by 40 cycles of 95°C for 5 s, 60°C for 30 s, and data collection, and then a final 65°C extension for 31 s, and a melt curve was produced. PCRs were normalized to *RPL13A*. All reactions yielded single-peak melt curves, confirming specificity. Amplification was sufficiently efficient to enable analysis of the PCR data using the ΔCt method. Primers were obtained from the references listed in table S2 or PrimerBank (https://pga.mgh.harvard.edu/primerbank/) (*51*, *52*).

Fluorescence microscopy

Immunofluorescence assays were performed on cells grown on four-chamber slides (Lab-Tek Chamber Slide, 177437, Thermo Fisher Scientific) according to assay-specific protocols. Cells were washed with PBS and fixed with 2 to 4% paraformaldehyde solution for 10 min with agitation at room temperature. Slides were washed three times each for at least 3 min with PBS and permeablized for 15 min with PBS/0.1% Trition X-100 with agitation at room temperature. Cells were then blocked for at least 20 min at room temperature or overnight at 4°C with 2% blocking solution [2% horse serum (Gibco), 2% goat serum (Gibco), 2% bovine serum albumin (BSA; A9647-500G, Sigma-Aldrich), 0.2% Triton X-100 (A16046, Alfa Aesar), and PBS to volume] with agitation at room temperature and were then probed overnight with antibodies specific to C1QBP (1:300; A302-862A, Bethyl Laboratories), DUX4 (1:50; clone P4H7, a gift from S. Tapscott), FUS (1:500; A300-293A, Bethyl Laboratories), dsRNA [1:300; SCICONS K1, English and Scientific Consulting, Hungary (SCICONS)], or γH2A.X (1:500; 05-636, Millipore) at 4°C with agitation. The following day, the cells were washed three times for at least 3 min each with PBS and were then incubated with a 1:300 dilution of an appropriate Alexa Fluor–conjugated secondary antibody (A11017, A11071, A11001, A21131, or A21123; Life Technologies) for at least 2 hours at room temperature with agitation. Cells were then incubated with Hoechst dye (1 μg/ml; B2261, Sigma-Aldrich) for at least 10 min at room temperature with agitation. Washes were repeated, and coverslips were mounted using Fluoro-Gel with tris (17985-11, Electron Microscopy Sciences). For HA immunofluorescence, cells were treated as above with the following modifications: Following the blocking step, hyaluronidase (HAase; ~4000 U/ml) from bovine testes (H3506, Sigma-Aldrich) in buffer [20 mM sodium phosphate buffer (pH 7.0), 77 mM NaCl, and 0.01% BSA] was diluted 1:10 in PBS for a final concentration of ~400 U/ml. Cells were in incubated in this HAase solution for 3 hours at 37°C with agitation. Cells were then washed in PBS and incubated in biotinylated HA-binding protein (10 μg/ml; 385911, Millipore/Sigma) diluted in PBS for 1 hour with agitation. Alexa Fluor 594–conjugated streptavidin (1:300; S32356, Life Technologies) was used in place of secondary antibody. For mitochondrial staining experiments, live cells were stained with 500 nM MitoSpy Orange CMTMRos (424803, BioLegend), washed with PBS, and then fixed and either washed and imaged immediately or immunostained as above. Images were collected using a Leica Microsystems DMR fluorescence microscope. For quantitative/cell counting experiments, randomness was ensured by viewing fields using phase-contrast optics and then switching to the relevant fluorescence optics. Nucleus and protein aggregate/distribution counts were determined by visual counts.

Cell death/apoptosis assays

To visualize DUX4-induced cell death, ~1.2×10^5 to 1.25×10^5 cells were plated on each well of a 12-well plate (353043, Falcon). The following day, the medium was replaced with medium containing the indicated compounds. After the indicated exposure time, cultures were visualized by phase-contrast microscopy using a Nikon Eclipse TS100 microscope.

To visualize caspase-3/7 activation, 5×10^4 cells per well were plated on four-chambered slides in 0.6 ml of media with or without DOX and either 30 μM InSolution Caspase-3 Inhibitor II (Z-DEVD-FMK; 264156, EMD/Millipore) or an equal volume of DMSO vehicle. After 23 hours, cells were stained by adding either two drops of ReadyProbes CellEvent Caspase-3/7 Green reagent (R37111, Invitrogen) per well or Hoechst dye (1 μg/ml), and the cultures were placed in the incubator for 1 hour. Cells were then imaged on a Nikon Eclipse TS100 microscope.

To quantitate apoptosis and cell death, 1.75×10^5 cells per well were plated on six-well plates. The next day, medium was replaced with medium containing the indicated compounds. After 24 hours, the medium was transferred to a 15-ml centrifuge tube. Wells were rinsed with PBS, which was transferred to the same tubes. Cells were then trypsinized with TrypLE Express (12605-010, Gibco), and reactions were stopped with an equal volume of media and added to the tubes. Wells were rinsed with PBS, which was also added to the tubes. The tubes were spun at ~400*g* for 5 min. The medium was removed, and the cells were suspended in PBS and then added to 5-ml flow cytometry tubes by passing through a 40-μm nylon strainer (352340, Falcon). Cells were then stained using the CellEvent Caspase-3/7 Green Flow Cytometry Assay Kit (C10427, Invitrogen) according to the manufacturer's instructions, with minor adjustments for volume. Flow cytometry was performed using a BD FACSCalibur instrument, and the data were analyzed using FlowJo software.

dsDNA break assay

dsDNA breaks were measured using the EMD/Millipore H2A.X Phosphorylation Assay Kit (17-344), according to the manufacturer's instructions with minor modifications for volume. Briefly, 1.75×10^5 MB135-DUX4i myoblasts were plated per well on six-well plates. The following day, the test compounds were added to the indicated concentrations. After 24 hours, the medium was transferred to 15-ml centrifuge tubes. Wells were rinsed with PBS, which was added to the centrifuge tubes. The cells were then trypsinized with TrypLE Express, and reactions were stopped with an equal volume of media and added to the tubes. Wells were washed with PBS, which was also added to the tubes. The tubes were then spun down at ~750*g* for 5 min and were washed three times with PBS. Cells were resuspended in 25 μl of fixation buffer and left on ice for 20 min. Fixed cells were spun down at ~10,000*g* and washed twice in PBS and then resuspended in 25 μl of permeablization buffer. Fluorescein isothiocyanate–conjugated antibody (1.75 μl) was then added, mixed, and left on ice for 20 min. Cells were then diluted with 100 μl of wash buffer, spun down, washed with Hanks' balanced salt solution (HBSS; 21-022-CV, Corning) and then resuspended in HBSS and transferred into a flow cytometry tube by passing through a 40-μm nylon strainer. Flow cytometry was then performed using a BD LSR II flow cytometer, and the data was analyzed using FlowJo software.

Mass spectrometry analysis

Co-IP experiments

Twenty-four hours after transfection with DUX4-expressing plasmids, co-IP experiments were performed as described [protocol 2.2 from (*53*)] except that lysis buffers were supplemented with protease inhibitor cocktail (2 μl/ml; P8340, Sigma-Aldrich). Cytoplasmic lysates were made with Tween 20 lysis buffer containing 25 mM tris-HCl (pH 8), 25 mM NaCl, 2 mM EDTA, 1 mM phenylmethylsulfonyl fluoride, and 0.5% Tween 20, and nuclear lysates were made with the same buffer containing 500 mM NaCl. Lysates were precleared with 2.5 μg of mouse immunoglobulin G (IgG) isotype control antibody (5415S, Cell Signaling Technology) and 30 μl of protein G Agarose beads (11719416001, Roche), and immunoprecipitation was performed with 15 μl of anti–DUX4 C-2 antibody (sc-376490, Santa Cruz Biotechnology) and 30 μl of Protein G Agarose beads (11719416001, Roche). Samples were boiled in 2X sample buffer [100 mM

tris, SDS (40 mg/ml), 20% glycerol, and 100 mM dithiothreitol] and were partially separated by polyacrylamide gel electrophoresis for about 2 cm into the gel. The gel was then stained with Imperial Protein Stain (24615, Thermo Fisher Scientific) according to the manufacturer's instructions. Lanes were then cut from the gel and submitted to the University of Massachusetts Medical School Proteomics core facility for analysis by mass spectrometry. Specific coimmunoprecipitating proteins were determined by enrichment of the product in pCI-Neo-DUX4 (*4*)–transfected myoblasts relative to pcDNA3.1-transfected 15ABicCT, 15BBicCT, or 15VBicCT myoblasts.

Sample preparation for mass spectrometry, liquid chromatography–tandem mass spectrometry analysis, and data analysis

Gel bands were cut into 1 mm by 1 mm pieces and placed in 1.5-ml Eppendorf tubes with 1 ml of water for 30 min. Samples were then prepared for mass spectrometry, and liquid chromatography–tandem mass spectrometry analysis was performed essentially as described (*54*). Data analysis was also performed as described except that raw data files were peak-processed with Proteome Discoverer (version 2.0, Thermo Fisher Scientific) before database searching with Mascot Server (version 2.4) against the Swissprot_Human database.

Co-IP/Western blot analysis

Nuclear lysates were prepared as for co-IP/mass spectrometry analysis except that lysates were precleared with 5 μg of mouse IgG_1 isotype control (02-6100, Thermo Fisher Scientific), and precipitations were performed with 4 μg of anti-DUX4 C-2 antibody or 4 μg of isotype control. Western blots were performed by separating samples on 12% Bolt Bis-Tris Plus precast gels (no. NW00122BOX, Thermo Fisher Scientific) in Mops buffer (NP0001-02, Invitrogen), transferring to polyvinylidene difluoride membranes, and probing according to standard methods. Blots were probed with 1:1000 dilutions of anti-C1QBP (A302-862A, Bethyl Laboratories) or anti-DUX4 clone E5-5 (ab124699, Abcam) antibodies, and enhanced chemiluminesence was performed using a mouse anti-rabbit–horseradish peroxidase secondary antibody (31464, Thermo Fisher Scientific), a SuperSignal West Femto kit (34094, Thermo Fisher Scientific) and a ChemiDoc MP Imaging system.

Statistical analysis

For all data presented in the figures, error bars are SEM except for colocalization experiments, where SDs are presented. Significance was determined using unpaired *t* tests for cases where the assumption of equal variance was appropriate or unpaired Welch's *t* tests where equal variance could not be assumed. The method used is indicated in each figure legend. Where indicated, *P* values were corrected for multiple hypothesis testing using the Bonferroni-Dunn method. Calculations were performed using GraphPad Prism software or GraphPad QuickCalcs (www.graphpad.com/quickcalcs/). Analysis was performed on the results of three independent experiments, as is traditional, except for RT-PCR experiments in Fig. 6, which, because of relatively small differences observed in preliminary experiments, were instead performed on six independent experiments. For all figures, $*P < 0.05$, $**P < 0.01$, $***P < 0.001$, and $****P \leq 0.0001$.

SUPPLEMENTARY MATERIALS

Supplementary material for this article is available at http://advances.sciencemag.org/cgi/content/full/5/12/eaaw7099/DC1

Fig. S1. DOX does not cause pathology in parental myoblasts.
Fig. S2. Inhibition of caspase-3/7 or ROS does not prevent C1QBP mislocalization.
Fig. S3. Compounds can provide resistance to DUX4-induced toxicity.
Fig. S4. DOX does not cause nuclear pathologies in parental myoblasts.
Fig. S5. FUS aggregates localize to sites of dsDNA breaks and are inhibited by 4MU.
Fig. S6. DNA damage does not cause accumulation of dsRNA after 24 hours and depends on 4MU.
Fig. S7. βME does not prevent DUX4-induced appearance of dsRNA foci.
Table S1. Cells used in this study.
Table S2. Primers used in this study.
Data S1. Identification of DUX4 copurifying proteins by mass spectrometry.

View/request a protocol for this paper from *Bio-protocol*.

REFERENCES AND NOTES

1. A. M. DeSimone, A. Pakula, A. Lek, C. P. Emerson Jr., Facioscapulohumeral Muscular Dystrophy. *Compr. Physiol.* **7**, 1229–1279 (2017).
2. P. G. Hendrickson, J. A. Doráis, E. J. Grow, J. L. Whiddon, J.-W. Lim, C. L. Wike, B. D. Weaver, C. Pflueger, B. R. Emery, A. L. Wilcox, D. A. Nix, C. M. Peterson, S. J. Tapscott, D. T. Carrell, B. R. Cairns, Conserved roles for murine DUX and human DUX4 in activating cleavage stage genes and MERVL/HERVL retrotransposons. *Nat. Genet.* **49**, 925–934 (2017).
3. L. de la Kethulle de Ryhove, E. Ansseau, C. Nachtegael, K. Pieters, C. Vanderplanck, M. Geens, K. Sermon, S. D. Wilton, F. Coppée, L. Lagneaux, A. Belayew, The Role of D4Z4-Encoded Proteins in the Osteogenic Differentiation of Mesenchymal Stromal Cells Isolated from Bone Marrow. *Stem Cells Dev.* **24**, 2674–2686 (2015).
4. J. Gabriëls, M.-C. Beckers, H. Ding, A. De Vriese, S. Plaisance, S. M. van der Maarel, G. W. Padberg, R. R. Frants, J. E. Hewitt, D. Collen, Nucleotide sequence of the partially deleted D4Z4 locus in a patient with FSHD identifies a putative gene within each 3.3 kb element. *Gene* **236**, 25–32 (1999).
5. L. N. Geng, Z. Yao, L. Snider, A. P. Fong, J. N. Cech, J. M. Young, S. M. van der Maarel, W. L. Ruzzo, R. C. Gentleman, R. Tawil, S. J. Tapscott, DUX4 Activates Germline Genes, Retroelements, and Immune Mediators: Implications for Facioscapulohumeral Dystrophy. *Dev. Cell* **22**, 38–51 (2012).
6. D. Bosnakovski, Z. Xu, E. J. Gang, C. L. Galindo, M. Liu, T. Simsek, H. R. Garner, S. Agha-Mohammadi, A. Tassin, F. Coppée, A. Belayew, R. R. Perlingeiro, M. Kyba, An isogenetic myoblast expression screen identifies DUX4-mediated FSHD-associated molecular pathologies. *EMBO J.* **27**, 2766–2779 (2008).
7. A. Dandapat, D. Bosnakovski, L. M. Hartweck, R. W. Arpke, K. A. Baltgalvis, D. Vang, J. Baik, R. Darabi, R. C. Perlingeiro, F. K. Hamra, K. Gupta, D. A. Lowe, M. Kyba, Dominant lethal pathologies in male mice engineered to contain an X-linked DUX4 transgene. *Cell Rep.* **8**, 1484–1496 (2014).
8. L. M. Wallace, S. E. Garwick, W. Mei, A. Belayew, F. Coppee, K. J. Ladner, D. Guttridge, J. Yang, S. Q. Harper, *DUX4*, a Candidate Gene for Facioscapulohumeral Muscular Dystrophy, Causes p53-Dependent Myopathy In Vivo. *Ann. Neurol.* **69**, 540–552 (2011).
9. V. Kowaljow, A. Marcowycz, E. Ansseau, C. B. Conde, S. Sauvage, C. Mattéotti, C. Arias, E. D. Corona, N. G. Nuñez, O. Leo, R. Wattiez, D. Figlewicz, D. Laoudj-Chenivesse, A. Belayew, F. Coppée, A. L. Rosa, The DUX4 gene at the FSHD1A locus encodes a pro-apoptotic protein. *Neuromuscul. Disord.* **17**, 611–623 (2007).
10. H. Mitsuhashi, S. Mitsuhashi, T. Lynn-Jones, G. Kawahara, L. M. Kunkel, Expression of DUX4 in zebrafish development recapitulates facioscapulohumeral muscular dystrophy. *Hum. Mol. Genet.* **22**, 568–577 (2013).
11. R. D. Wuebbles, S. W. Long, M. L. Hanel, P. L. Jones, Testing the effects of FSHD candidate gene expression in vertebrate muscle development. *Int. J. Clin. Exp. Pathol.* **3**, 386–400 (2010).
12. A. M. Rickard, L. M. Petek, D. G. Miller, Endogenous DUX4 expression in FSHD myotubes is sufficient to cause cell death and disrupts RNA splicing and cell migration pathways. *Hum. Mol. Genet.* **24**, 5901–5914 (2015).
13. D. Bosnakovski, M. D. Gearhart, E. A. Toso, O. O. Recht, A. Cucak, A. K. Jain, M. C. Barton, M. Kyba, p53-independent DUX4 pathology in cell and animal models of facioscapulohumeral muscular dystrophy. *Dis. Model. Mech.* **10**, 1211–1216 (2017).
14. S. C. Shadle, J. W. Zhong, A. E. Campbell, M. L. Conerly, S. Jagannathan, C.-J. Wong, T. D. Morello, S. M. van der Maarel, S. J. Tapscott, DUX4-induced dsRNA and MYC mRNA stabilization activate apoptotic pathways in human cell models of facioscapulohumeral dystrophy. *PLOS Genet.* **13**, e1006658 (2017).
15. S. T. Winokur, K. Barrett, J. H. Martin, J. R. Forrester, M. Simon, R. Tawil, S. A. Chung, P. S. Masny, D. A. Figlewicz, Facioscapulohumeral muscular dystrophy (FSHD) myoblasts demonstrate increased susceptibility to oxidative stress. *Neuromuscul. Disord.* **13**, 322–333 (2003).
16. P. Dmitriev, Y. B. Saada, C. Dib, E. Ansseau, A. Barat, A. Hamade, P. Dessen, T. Robert, V. Lazar, R. A. N. Louzada, C. Dupuy, V. Zakharova, G. Carnac, M. Lipinski, Y. S. Vassetzky, DUX4-induced constitutive DNA damage and oxidative stress contribute to aberrant differentiation of myoblasts from FSHD patients. *Free Radic. Biol. Med.* **99**, 244–258 (2016).
17. A. Turki, M. Hayot, G. Carnac, F. Pillard, E. Passerieux, S. Bommart, E. R. de Mauverger, G. Hugon, J. Pincemail, S. Pietri, K. Lambert, A. Belayew, Y. Vassetzky, R. J. Morales, J. Mercier, D. Laoudj-Chenivesse, Functional muscle impairment in facioscapulohumeral muscular dystrophy is correlated with oxidative stress and mitochondrial dysfunction. *Free Radic. Biol. Med.* **53**, 1068–1079 (2012).

18. B. Celegato, D. Capitanio, M. Pescatori, C. Romualdi, B. Pacchioni, S. Cagnin, A. Viganò, L. Colantoni, S. Begum, E. Ricci, R. Wait, G. Lanfranchi, Parallel protein and transcript profiles of FSHD patient muscles correlate to the D4Z4 arrangement and reveal a common impairment of slow to fast fibre differentiation and a general deregulation of MyoD-dependent genes. *Proteomics* **6**, 5303–5321 (2006).
19. M. Barro, G. Carnac, S. Flavier, J. Mercier, Y. Vassetzky, D. Laoudj-Chenivesse, Myoblasts from affected and non-affected FSHD muscles exhibit morphological differentiation defects. *J. Cell. Mol. Med.* **14**, 275–289 (2010).
20. C. Vanderplanck, E. Ansseau, S. Charron, N. Stricwant, A. Tassin, D. Laoudj-Chenivesse, S. D. Wilton, F. Coppée, A. Belayew, The FSHD Atrophic Myotube Phenotype Is Caused by DUX4 Expression. *PLOS ONE* **6**, e26820 (2011).
21. P. Dmitriev, E. Kiseleva, O. Kharchenko, E. Ivashkin, A. Pichugin, P. Dessen, T. Robert, F. Coppée, A. Belayew, G. Carnac, D. Laoudj-Chenivesse, M. Lipinski, A. Vasiliev, Y. S. Vassetzky, Dux4 controls migration of mesenchymal stem cells through the Cxcr4-Sdf1 axis. *Oncotarget* **7**, 65090–65108 (2016).
22. D. Bosnakovski, E. A. Toso, L. M. Hartweck, A. Magli, H. A. Lee, E. R. Thompson, A. Dandapat, R. C. R. Perlingeiro, M. Kyba, The DUX4 homeodomains mediate inhibition of myogenesis and are functionally exchangeable with the Pax7 homeodomain. *J. Cell Sci.* **130**, 3685–3697 (2017).
23. C. R. S. Banerji, M. Panamarova, H. Hebaishi, R. B. White, F. Relaix, S. Severini, P. S. Zammit, PAX7 target genes are globally repressed in facioscapulohumeral muscular dystrophy skeletal muscle. *Nat. Commun.* **8**, 2152 (2017).
24. P. Haynes, K. Kernan, S.-L. Zhou, D. G. Miller, Expression patterns of FSHD-causing DUX4 and myogenic transcription factors PAX3 and PAX7 are spatially distinct in differentiating human stem cell cultures. *Skelet. Muscle* **7**, 13 (2017).
25. Q. Feng, L. Snider, S. Jagannathan, R. Tawil, S. M. van der Maarel, S. J. Tapscott, R. K. Bradley, A feedback loop between nonsense-mediated decay and the retrogene DUX4 in facioscapulohumeral muscular dystrophy. *eLife* **4**, e04996 (2015).
26. S. Homma, M. L. Beermann, F. M. Boyce, J. B. Miller, Expression of FSHD-related DUX4-FL alters proteostasis and induces TDP-43 aggregation. *Ann. Clin. Transl. Neurol.* **2**, 151–166 (2015).
27. A. Tassin, B. Leroy, D. Laoudj-Chenivesse, A. Wauters, C. Vanderplanck, M.-C. Le Bihan, F. Coppée, R. Wattiez, A. Belayew, FSHD Myotubes with Different Phenotypes Exhibit Distinct Proteomes. *PLOS ONE* **7**, e51865 (2012).
28. S. Homma, M. L. Beermann, B. Yu, F. M. Boyce, J. B. Miller, Nuclear bodies reorganize during myogenesis in vitro and are differentially disrupted by expression of FSHD-associated DUX4. *Skelet. Muscle* **6**, 42 (2016).
29. E. Ansseau, J. O. Eidahl, C. Lancelot, A. Tassin, C. Matteotti, C. Yip, J. Liu, B. Leroy, C. Hubeau, C. Gerbaux, S. Cloet, A. Wauters, S. Zorbo, P. Meyer, I. Pirson, D. Laoudj-Chenivesse, R. Wattiez, S. Q. Harper, A. Belayew, F. Coppée, Homologous Transcription Factors DUX4 and DUX4c Associate with Cytoplasmic Proteins during Muscle Differentiation. *PLOS ONE* **11**, e0146893 (2016).
30. C. M. Rao, T. B. Deb, S. Gupta, K. Datta, Regulation of cellular phosphorylation of hyaluronan binding protein and its role in the formation of second messenger. *Biochim. Biophys. Acta Gen. Subj.* **1336**, 387–393 (1997).
31. M. Majumdar, J. Meenakshi, S. K. Goswami, K. Datta, Hyaluronan binding protein 1 (HABP1)/C1QBP/p32 Is an endogenous substrate for MAP kinase and is translocated to the nucleus upon mitogenic stimulation. *Biochem. Biophys. Res. Commun.* **291**, 829–837 (2002).
32. T. B. Deb, K. Datta, Molecular Cloning of Human Fibroblast Hyaluronic Acid-binding Protein Confirms Its Identity with P-32, a Protein Co-purified with Splicing Factor SF2: Hyaluronic acid-binding protein as p-32 protein, co-purified with splicing factor SF2. *J. Biol. Chem.* **271**, 2206–2212 (1996).
33. S. Jagannathan, S. C. Shadle, R. Resnick, L. Snider, R. N. Tawil, S. M. van der Maarel, R. K. Bradley, S. J. Tapscott, Model systems of DUX4 expression recapitulate the transcriptional profile of FSHD cells. *Hum. Mol. Genet.* **25**, 4419–4431 (2016).
34. T. I. Jones, J. C. J. Chen, F. Rahimov, S. Homma, P. Arashiro, M. L. Beermann, O. D. King, J. B. Miller, L. M. Kunkel, C. P. Emerson, K. R. Wagner, P. L. Jones, Facioscapulohumeral muscular dystrophy family studies of DUX4 expression: evidence for disease modifiers and a quantitative model of pathogenesis. *Hum. Mol. Genet.* **21**, 4419–4430 (2012).
35. L. Snider, L. N. Geng, R. J. L. F. Lemmers, M. Kyba, C. B. Ware, A. M. Nelson, R. Tawil, G. N. Filippova, S. M. van der Maarel, S. J. Tapscott, D. G. Miller, Facioscapulohumeral Dystrophy: Incomplete Suppression of a Retrotransposed Gene. *PLOS Genet.* **6**, e1001181 (2010).
36. N. Nagy, H. F. Kuipers, A. R. Frymoyer, H. D. Ishak, J. B. Bollyky, T. N. Wight, P. L. Bollyky, 4-Methylumbelliferone treatment and hyaluronan inhibition as a therapeutic strategy in inflammation, autoimmunity, and cancer. *Front. Immunol.* **6**, 123 (2015).
37. C. Chattopadhyay, D. Hawke, R. Kobayashi, S. N. Maity, Human p32, interacts with B subunit of the CCAAT-binding factor, CBF/NF-Y, and inhibits CBF-mediated transcription activation in vitro. *Nucleic Acids Res.* **32**, 3632–3641 (2004).
38. L. Yu, Z. Zhang, P. M. Loewenstein, K. Desai, Q. Tang, D. Mao, J. S. Symington, M. Green, Molecular cloning and characterization of a cellular protein that interacts with the human immunodeficiency virus type 1 Tat transactivator and encodes a strong transcriptional activation domain. *J. Virol.* **69**, 3007–3016 (1995).
39. P. Saha, K. Datta, Multi-functional, multicompartmental hyaluronan-binding protein 1 (HABP1/p32/gC1qR): implication in cancer progression and metastasis. *Oncotarget* **9**, 10784–10807 (2018).
40. V. Fogal, A. D. Richardson, P. P. Karmali, I. E. Scheffler, J. W. Smith, E. Ruoslahti, Mitochondrial p32 Protein Is a Critical Regulator of Tumor Metabolism via Maintenance of Oxidative Phosphorylation. *Mol. Cell. Biol.* **30**, 1303–1318 (2010).
41. A. M. McGee, D. L. Douglas, Y. Liang, S. M. Hyder, C. P. Baines, The mitochondrial protein C1qbp promotes cell proliferation, migration and resistance to cell death. *Cell Cycle* **10**, 4119–4127 (2011).
42. L. C. Hunt, C. Gorman, C. Kintakas, D. R. McCulloch, E. J. Mackie, J. D. White, Hyaluronan synthesis and myogenesis: a requirement for hyaluronan synthesis during myogenic differentiation independent of pericellular matrix formation. *J. Biol. Chem.* **288**, 13006–13021 (2013).
43. Y. Bou Saada, C. Dib, P. Dmitriev, A. Hamade, G. Carnac, D. Laoudj-Chenivesse, M. Lipinski, Y. S. Vassetzky, Facioscapulohumeral dystrophy myoblasts efficiently repair moderate levels of oxidative DNA damage. *Histochem. Cell Biol.* **145**, 475–483 (2016).
44. W.-Y. Wang, L. Pan, S. C. Su, E. J. Quinn, M. Sasaki, J. C. Jimenez, I. R. A. Mackenzie, E. J. Huang, L.-H. Tsai, Interaction of FUS and HDAC1 Regulates DNA Damage Response and Repair in Neurons. *Nat. Neurosci.* **16**, 1383–1391 (2013).
45. B. R. Hawley, W.-T. Lu, A. Wilczynska, M. Bushell, The emerging role of RNAs in DNA damage repair. *Cell Death Differ.* **24**, 580–587 (2017).
46. L. J. Kuo, L.-X. Yang, γ-H2AX - A Novel Biomarker for DNA Double-strand Breaks. *In Vivo* **22**, 305–309 (2008).
47. C. Vanderplanck, A. Tassin, E. Ansseau, S. Charron, A. Wauters, C. Lancelot, K. Vancutsem, D. Laoudj-Chenivesse, A. Belayew, F. Coppée, Overexpression of the double homeodomain protein DUX4c interferes with myofibrillogenesis and induces clustering of myonuclei. *Skelet. Muscle* **8**, 2 (2018).
48. C. R. Giesige, L. M. Wallace, K. N. Heller, J. O. Eidahl, N. Y. Saad, A. M. Fowler, N. K. Pyne, M. Al-Kharsan, A. Rashnonejad, G. A. Chermahini, J. S. Domire, D. Mukweyi, S. E. Garwick-Coppens, S. M. Guckes, K. J. McLaughlin, K. Meyer, L. R. Rodino-Klapac, S. Q. Harper, AAV-mediated follistatin gene therapy improves functional outcomes in the TIC-DUX4 mouse model of FSHD. *JCI Insight* **3**, e123538 (2018).
49. D. Vigetti, E. Karousou, M. Viola, S. Deleonibus, G. De Luca, A. Passi, Hyaluronan: Biosynthesis and signaling. *Biochim. Biophys. Acta* **1840**, 2452–2459 (2014).
50. G. Stadler, F. Rahimov, O. D. King, J. C. J. Chen, J. D. Robin, K. R. Wagner, J. W. Shay, C. P. Emerson Jr., W. E. Wright, Telomere position effect regulates DUX4 in human facioscapulohumeral muscular dystrophy. *Nat. Struct. Mol. Biol.* **20**, 671–678 (2013).
51. A. Spandidos, X. Wang, H. Wang, B. Seed, PrimerBank: A resource of human and mouse PCR primer pairs for gene expression detection and quantification. *Nucleic Acids Res.* **38**, D792–D799 (2010).
52. X. Wang, A. Spandidos, H. Wang, B. Seed, PrimerBank: A PCR primer database for quantitative gene expression analysis, 2012 update. *Nucleic Acids Res.* **40**, D1144–D1149 (2012).
53. E. Klenova, I. Chernukhin, T. Inoue, S. Shamsuddin, J. Norton, Immunoprecipitation techniques for the analysis of transcription factor complexes. *Methods* **26**, 254–259 (2002).
54. R. Ganesan, J. Leszyk, A. Jacobson, Selective profiling of ribosomes associated with yeast Upf proteins. *Methods* **155**, 58–67 (2019).

Acknowledgments: We would like to thank S. Tapscott for providing us with several reagents used in this study, including the MB135-DUX4i cell line and DUX4 antibodies; G. Stadler and W. E. Wright for providing immortalized cell lines; and J. Chen, L. Hayward, R. Gerstein, and Z. Matijasevic for helpful suggestions and/or technical support. **Funding:** This work was supported by the FSH Society grant FSHS-82015-05 to A.M.D. and a travel grant to A.M.D. from the FSH Society Ed and Betty Schechter Memorial Research Fund and by the Wellstone Center for FSH research and NIH/National Institute of Child Health and Human Development grant U54HD0060848 to C.P.E. **Author contributions:** A.M.D. and C.P.E. conceived experiments. A.M.D. performed all experiments except the mass spectrometry analysis, which was performed by J.L. K.W. developed FSHD cell lines. A.M.D. and C.P.E. wrote the paper. **Competing interests:** The authors declare that they have no competing interests. **Data and materials availability:** All data needed to evaluate the conclusions in the paper are present in the paper and/or the Supplementary Materials. Additional data related to this paper may be requested from the authors.

Submitted 18 January 2019
Accepted 23 October 2019
Published 11 December 2019
10.1126/sciadv.aaw7099

Citation: A. M. DeSimone, J. Leszyk, K. Wagner, C. P. Emerson Jr., Identification of the hyaluronic acid pathway as a therapeutic target for facioscapulohumeral muscular dystrophy. *Sci. Adv.* **5**, eaaw7099 (2019).